

Influence of vertical heat exchanger tubes, their arrangement and the column diameter on the hydrodynamics in a gas–solid bubbling fluidized bed

Schillinger, Frank; Maurer, Simon; Wagner, Evert C.; van Ommen, J. Ruud; Mudde, Robert F.; Schildhauer, Tilman J.

DOI

[10.1016/j.ijmultiphaseflow.2017.07.013](https://doi.org/10.1016/j.ijmultiphaseflow.2017.07.013)

Publication date

2017

Document Version

Final published version

Published in

International Journal of Multiphase Flow

Citation (APA)

Schillinger, F., Maurer, S., Wagner, E. C., van Ommen, J. R., Mudde, R. F., & Schildhauer, T. J. (2017). Influence of vertical heat exchanger tubes, their arrangement and the column diameter on the hydrodynamics in a gas–solid bubbling fluidized bed. *International Journal of Multiphase Flow*, 97, 46-59. <https://doi.org/10.1016/j.ijmultiphaseflow.2017.07.013>

Important note

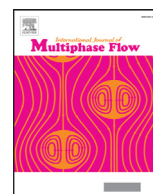
To cite this publication, please use the final published version (if applicable). Please check the document version above.

Copyright

Other than for strictly personal use, it is not permitted to download, forward or distribute the text or part of it, without the consent of the author(s) and/or copyright holder(s), unless the work is under an open content license such as Creative Commons.

Takedown policy

Please contact us and provide details if you believe this document breaches copyrights. We will remove access to the work immediately and investigate your claim.



Influence of vertical heat exchanger tubes, their arrangement and the column diameter on the hydrodynamics in a gas–solid bubbling fluidized bed



Frank Schillinger^a, Simon Maurer^a, Evert C. Wagner^b, J. Ruud van Ommen^b, Robert F. Mudde^b, Tilman J. Schildhauer^{a,*}

^a Paul Scherrer Institute, 5232 Villigen PSI, Switzerland

^b Delft University of Technology, Van der Maasweg 9, 2629 HZ Delft, The Netherlands

ARTICLE INFO

Article history:

Received 18 January 2017

Revised 14 July 2017

Accepted 17 July 2017

Available online 20 July 2017

Keywords:

X-ray measurements
Bubbling fluidized bed
Vertical internals
Bubble properties
Bubble distribution
Scale-up

ABSTRACT

The hydrodynamic behavior of a cold-flow gas–solid fluidized bed with an inner diameter of 22 cm is investigated by means of an ultra-fast X-ray tomographic setup. In the case of an exothermal reaction, heat exchanger tubes are required to remove the reaction heat out of the bubbling fluidized bed reactor. For the examined cold-flow model, the heat exchanger tubes are replaced by vertical internals that serve as placeholder. The influence of vertical internals on the bubble properties for different spatial configurations (square and circular arrangements) is investigated in addition to measurements without internals. Furthermore, the hydrodynamic results of the Ø 22 cm column are compared with an available data set which is based on measurements that were conducted in a column with an inner diameter of 14 cm. The objective of this paper is to provide measurement data for the scale-up process as well as for various computer models simulating a bubbling fluidized bed with vertical internals. It was found that the scale-up process from pilot plants to an industrial scale may be simplified if vertical internals are present, independently of the geometric arrangement.

© 2017 Elsevier Ltd. All rights reserved.

1. Introduction

Fluidized beds can be operated in a broad range of fluidization states as shown in [Yerushalmi and Cankurt \(1979\)](#). One possible operation mode is the bubbling regime for which the volume flow of gas is adjusted such that voids are formed near the distributor plate and rise as so-called bubbles through the bed ([Kunii and Levenspiel, 1968](#)). In case of a bubbling fluidized bed reactor (BFB)¹, the reactor performance mainly depends on the bubble size (BS)² and the bubble rise velocity (BRV)³, since both, the particle mixing as well as the gas mixing, are influenced by those properties ([Valenzuela and Glicksman, 1985](#); [Latham and Pottert, 1970](#)). The overall reaction rate may be controlled by the gas exchange from the bubble phase into the dense phase where the majority of the catalyst particles is located ([Beetstra et al., 2009](#)). In particular for strongly exothermic reactions under pressure, also the

heat removal is a limiting factor for the reactor design. This is due to the fact that a higher pressure accelerates the reaction resulting in a larger heat production per volume. Bubbling fluidized bed reactors are a well suited reactor type for strongly exothermic reactions. The high degree of particle mixing entails a heat transfer from high temperature to low temperature regions, so that local hotspots that are commonly in regions of high conversion are attenuated ([Kunii and Levenspiel, 2013](#)). In order to enhance the heat removal, the heat transfer area can be increased with vertical or horizontal internals that are located inside the BFB and serve as heat exchanger tubes ([Staub, 1979](#); [Kim et al., 2003](#); [Gunn and Hlal, 1996](#); [Natale et al., 2010](#)).

Amongst other measurement techniques like optical probes ([Acosta-Iborra et al., 2011](#); [Rüdisüli et al., 2012](#)), capacitive probes ([Rautenbach et al., 2013](#)) or pressure fluctuation measurements ([Acosta-Iborra et al., 2011](#); [van Ommen and Mudde, 2007](#)), the hydrodynamics can be determined by means of an ultra-fast X-ray setup ([Mudde, 2011](#); [Whitemarsh et al., 2016](#)). As investigated in [Maurer et al. \(2015\)](#), vertical internals lead to smaller mean bubble size and bubble rise velocity which is favorable for the mass transfer in BFB reactors. Common literature correlations for the dependence between BS and BRV ([Kunii and Levenspiel, 1968](#)) of

* Corresponding author.

E-mail address: tilman.schildhauer@psi.ch (T.J. Schildhauer).

¹ BFB: Bubbling fluidized bed.

² BS: Bubble size.

³ BRV: Bubble rise velocity.

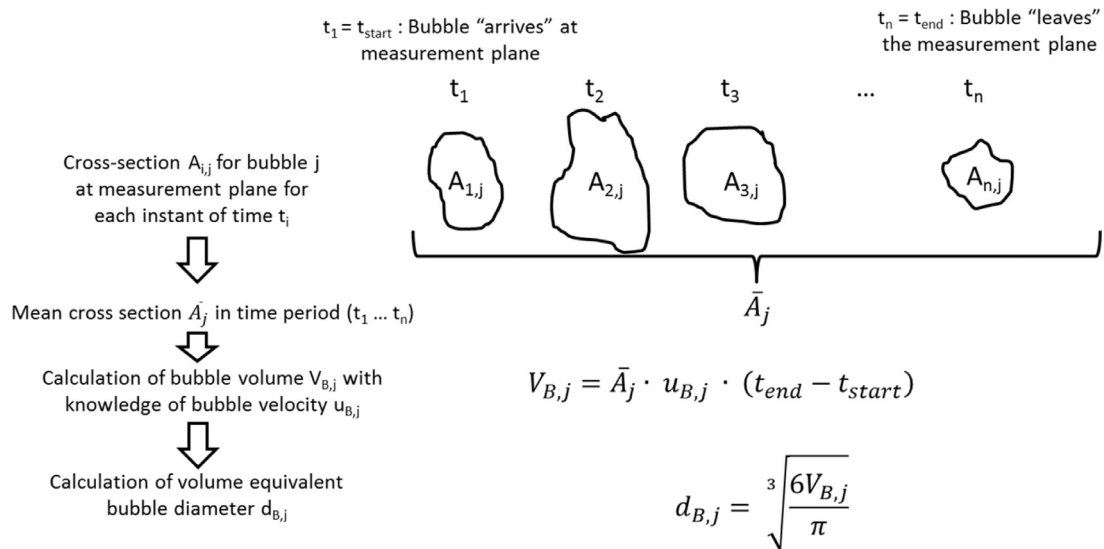


Fig. 1. Procedure to determine the bubble volume (equivalent diameter) based on the reconstructed images of a certain bubble at a measurement plane.

ten do not describe the bubble properties in a satisfactory way for a system with vertical internals as pointed out in Maurer et al. (2015) and Rüdüsüli et al. (2012). Therefore, these correlations are not sufficient to support the scale-up process of bubbling fluidized beds. So, further knowledge about the hydrodynamic state in a BFB with vertical internals is essential for both the development of a reactor model and a proper scale-up from lab-scale over pilot-scale to an industrial-scale reactor (Glicksman, 1984).

To enlarge the database for bubbling fluidized beds with internals, further X-ray measurements have been conducted in the scope of Maurer (2015) at a BFB with an inner diameter of 22 cm. Scale-up of fluidized beds proves to be a challenging task for engineers (Knowlton et al., 2005). To support the scale-up process, experiments with a bubbling fluidized bed in different dimensions are necessary to close the gap from a laboratory scale towards an industrial scale that may lie in the range from one to several meters (Werther, 1974; Baskakov et al., 1986). The generated data (from Maurer et al., 2015; Maurer, 2015) form the base for a correlation which was derived in Maurer et al. (2016) to correlate the bubble size and bubble velocity distribution in a BFB with vertical internals and an inner diameter of 14, respectively, 22 cm. Within the scope of the present paper, the influence of different internals arrangements on the bubble properties, the bubble hold-up and centroid distribution for the column of 22 cm in diameter are reported. Furthermore, these data are compared with a dataset for a column with a diameter of 14 cm.

2. Experimental

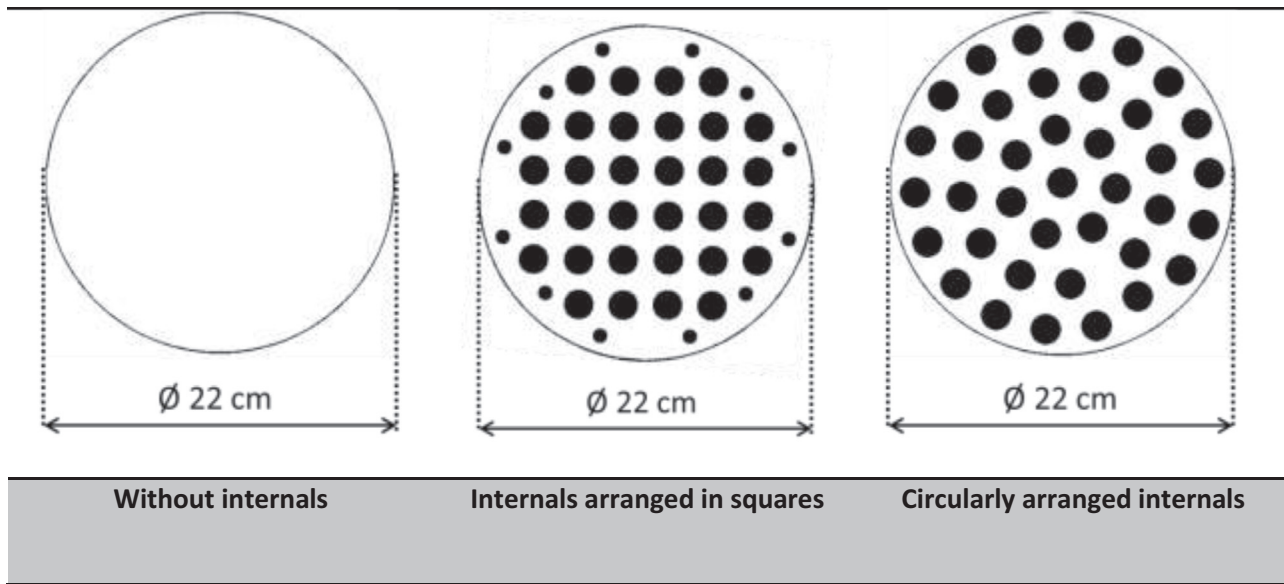
All hydrodynamic experiments were conducted with a fast X-ray tomographic scanner located at Delft University of Technology at ambient pressure and temperature in the scope of Maurer (2015). Air was used as fluidization medium. The tomographic setup consists of three X-ray point sources and a total of six detector arrays each with 32 detectors. The detector arrays are located circularly around the column in two rings with a vertical distance of 40 mm. This experimental setup leads to a mean distance of 1.86 cm between the X-ray beams that reach the upper and lower detector array rings (referred to in this paper as measurement planes). The intensity of the X-ray radiation on each detector is measured with a frequency of 2500 Hz and used as signal for the further data processing. A detailed description of the

measurement setup is given in Mudde (2011) and Mudde (2010). All measurements were conducted for a length of two minutes to obtain a representative number of bubbles for a statistically significant evaluation of the bubble data.

The intensity of each detector is converted into a path length occupied by air. The image reconstruction of the fluidization state at the measurement plane is conducted for each time of measurement with the simultaneous algebraic reconstruction technique (SART) (Andersen and Kak, 1984). The reconstructed slices have a resolution of 55×55 pixels in the horizontal direction. In order to reduce the computing time, the mean of 10 consecutive measurements was taken which results in an effective temporal resolution of 250 Hz. Details of the image reconstruction process are described in Mudde (2011) and Maurer (2015).

The bubble rise velocity is determined by the time difference the center of gravity of a bubble needs to pass the lower and the upper measurement plane. In the scope of this study, an improved approach is presented to determine the bubble volume and the volume equivalent bubble diameter out of a series of 2-D images (see Fig. 1). The bubble volume can be determined based on the average cross-section of a bubble at the measurement plane, the time period a bubble is present at the measurement plane and the bubble rise velocity. In the next step, the bubble volume V_B is used to calculate the diameter $d_{b,eq}$ of a sphere corresponding to the volume V_B .

Alumina particles (manufacturer Puralox® NWa-155) with a Sauter mean diameter of $289 \mu\text{m}$ and a density of 1350 kg/m^3 were used as bed material. A detailed particle characterization is given in Rüdüsüli (2012). All measurements were performed successively for a setup without internals, a setup with internals arranged in squares and a setup with internals arranged in a circular pattern. The minimum fluidization velocity u_{mf} was determined to be 3 cm/s (Maurer et al., 2014). The cross-section of the investigated columns with the respective internal arrangement is shown in Table 1 whilst the cavity inside the internals was filled with bed material for the experiments. The column has an inner diameter of 22 cm; the tubes inside the column have an outer diameter of 2 cm. Smaller tubes of 1 cm are located between the outer row of the tubes and the wall to fill the empty space for the setup in which the internals are arranged in squares. For all configurations with vertical internals, two tubes are connected by a "U-connector" to mimic the real shape of the internals (see Fig. 2). The bottom

Table 1Cross-section of the investigated internals configurations for the \varnothing 22 cm column.

of the “U-connector” is located at a height of 3 cm above the distributor plate which means that the first 3 cm of the bed are free of internals. At the top of the column, the internals are fixed between two flanges by a grid pattern that corresponds to the particular internal design to keep the distance of 3 cm between the “U-connectors” and the distributor plate.

A porous sinter metal plate with a thickness of 3 mm and a pore size of $10\ \mu\text{m}$ served as the gas distributor. The measured pressure drop above the distributor plate is given in the Appendix of this work (see Fig. 20), the pressure drop above the bed is in the range of 40 mbar. In general, the influence of the distributor plate and the design of the windbox on the fluidization is negligible if the pressure drop across the bed is not larger than the pressure drop across the distributor plate (Sasic et al., 2005) which is the case for the investigated system.

In order to obtain comparable results for different internals arrangements, the fluidization number u/u_{mf} was taken as reference parameter. The fluidization number u/u_{mf} describes the ratio between the actual gas velocity and the gas velocity at minimum fluidization conditions and was taken as reference parameter to

compare the results obtained at the different geometries of internals. To achieve an identical fluidization number, the total gas flow was adapted depending on the number of internals. Hence, for the same fluidization number, the ratio between the total volume flow of air and the area free of internals remains constant for all configurations. At the column with a diameter of 22 cm, the measurements were conducted at the fluidization numbers and measurement heights above the distributor plate as depicted in Table 3 for all arrangements of internals. The measurements at the column with a diameter of 14 cm (see Table 2) were only conducted up to a fluidization number of 4 and a measurement height of 46 cm. For both column diameters, the static bed height of 60 cm was kept constant for all fluidization numbers and measurement heights.

3. Results

3.1. Bubble images

The high temporal resolution of the X-ray measurement setup enables a quasi-three-dimensional reconstruction of the bubbles. To visualize the bubbles, the reconstructed images of one measurement plane are stacked on top of each other for all consecutive measurement points. For a fluidization number of three and a measurement height of 36 cm, the reconstructed bubbles are shown in Fig. 3 for all types of internals arrangements. The internals are not depicted in the figures. Yet, their location is indicated by the surface of the reconstructed bubbles that surround the internals. The thickness of all slides in z-direction is selected such that bubbles rising with the mean BRV are neither elongated nor compressed. Since the mean bubble rise velocity depends both on the internals configuration as well as on the fluidization number, the thickness of a slice is individual for each reconstruction.

The quasi-three-dimensional reconstruction depicts that bubbles in a setup with vertical internals show a much more uneven surface compared to the setup without internals for which the bubbles appear in a rather round shape. Furthermore, the presence of internals seems to reduce the bubble volume and to increase the bubble number. Similar results have already been reported for a BFB with an inner diameter of 14 cm in Maurer et al. (2015). With regard to the mass transfer from the bubble phase into the dense



Fig. 2. Picture of “U-connectors” (configuration: internals arranged in squares).

Table 2
Cross-section of the investigated internals configurations for the \varnothing 14 cm column.

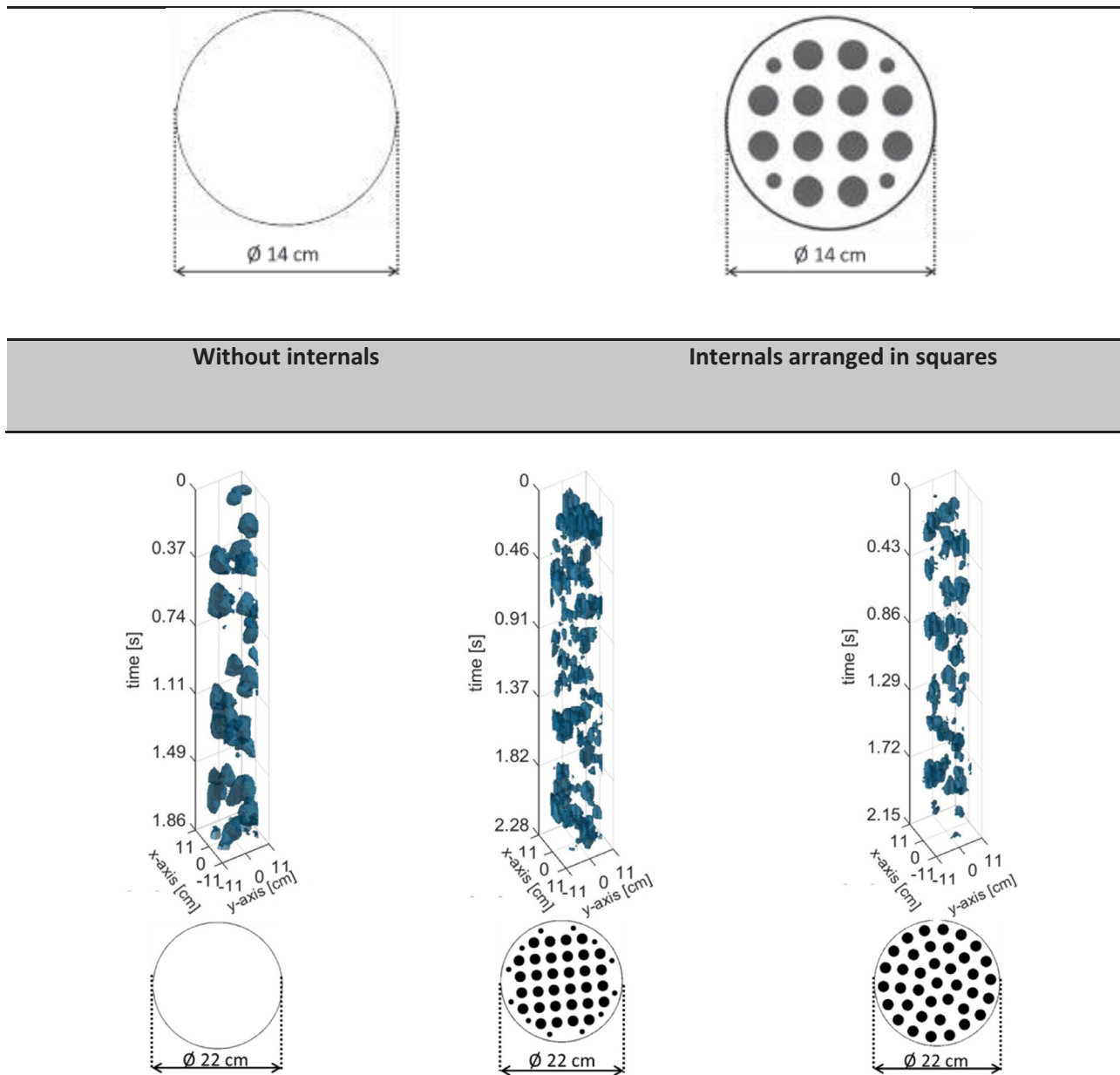


Fig. 3. Reconstructed bubbles at a measurement height of 36 cm and a fluidization number of three.

Table 3
Analyzed fluidization numbers and measurement heights.

u/u_{mf} [dimensionless]	1.5	2	3	4	6
X-ray height [cm]	16	26	36	46	56

phase, smaller bubbles are preferred due to a higher ratio of bubble surface to bubble volume. Fig. 4 presents the reconstructed pictures for a fluidization number of six at a measurement height of again 36 cm.

For a fluidization number of six, the effect of vertical internals is even more obvious. Whereas undesired slugs are visible for the setting without internals, the formation of slugs is less pronounced if vertical internals are present. Similar findings have already been reported for a column with a diameter of 14 cm by means of pres-

sure fluctuation measurements and optical probing in the scope of Rüdüsüli et al. (2012).

3.2. Hold-up and bubble centroid distribution

The bubble hold-up distribution over the cross-section is an important design parameter for all kind of multiphase flow systems (Kumar et al., 1997). Preferential pathways of bubbles inside a BFB are undesired since in regions with a lower bubble activity, the degree of solid mixing is reduced. Especially in a bubbling fluidized bed reactor, a proper solid mixing is the basis for the internal catalyst regeneration as examined in Kopyscinski et al. (2009) and Seemann et al. (2006). The evaluation of X-ray tomographic data allows the determination of a time-averaged bubble hold-up distribution over the measurement period. Furthermore, the location of the bubble centroid may be determined by means of the vol-

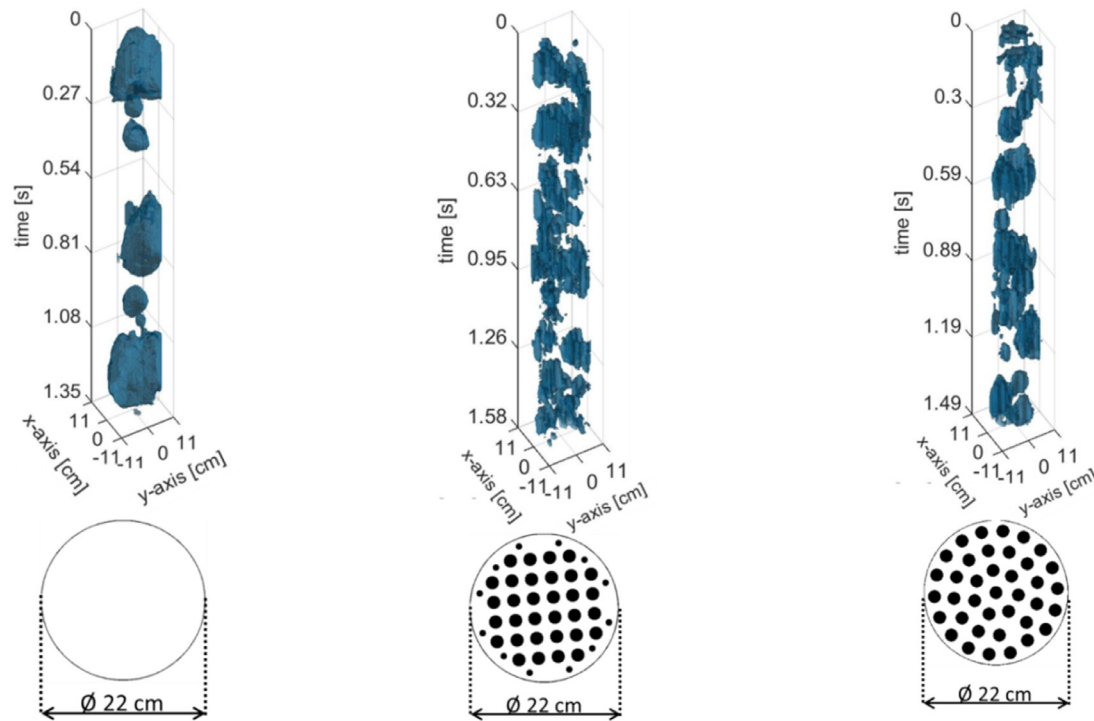


Fig. 4. Reconstructed bubbles at a measurement height of 36 cm and a fluidization number of six.

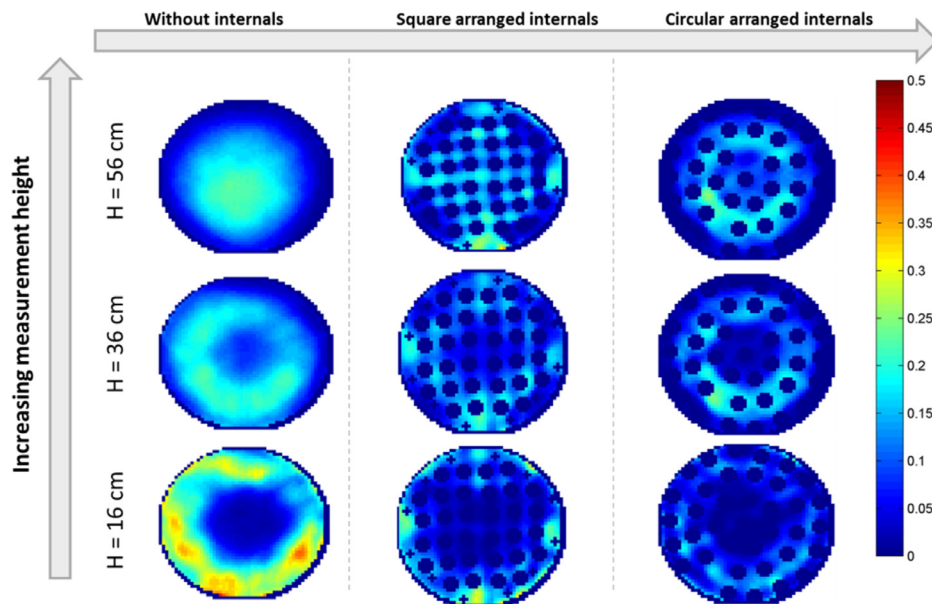


Fig. 5. Hold-up distribution at different measurement heights for a fluidization number of three, \varnothing column = 22 cm.

umetric center of gravity. The distribution of the bubble centroid positions on the cross-section may also be used as an indicator to judge if the bubbles are distributed uniformly which is conducive for an optimal reactor performance.

3.2.1. Hold-up evaluation for a fluidization number of three

Fig. 5 shows the hold-up distribution for all investigated internals at a measurement height of 16 cm, 36 cm and 56 cm and a fluidization number of three.

For a fluidization number of three, only the setup without internals at a measurement height of 16 cm shows locally limited hold-up values of up to 40%. The measurements without internals show a region of a higher hold-up that has the shape of a circular ring

which contracts for increasing bed heights. The phenomenon that the bubbles are concentrated next to the wall in the lower regions of the bed has already been described in and was illustrated by experiments at a fluidized bed with a diameter of 14 cm in Maurer et al. (2015). For circularly arranged internals, the area with an increased hold-up also shows an annular shape, although the hold-up is significantly lower compared to the setup without internals. For the internals arranged in squares, regions with an increased hold-up are located in the area near the wall where no small tubes are present. The missing tubes could facilitate the bubble rising in this region which leads to a higher hold-up, however, without exceeding a maximum value of 30% in these areas. Furthermore, the hold-up for the setup with quadratically arranged internals seems

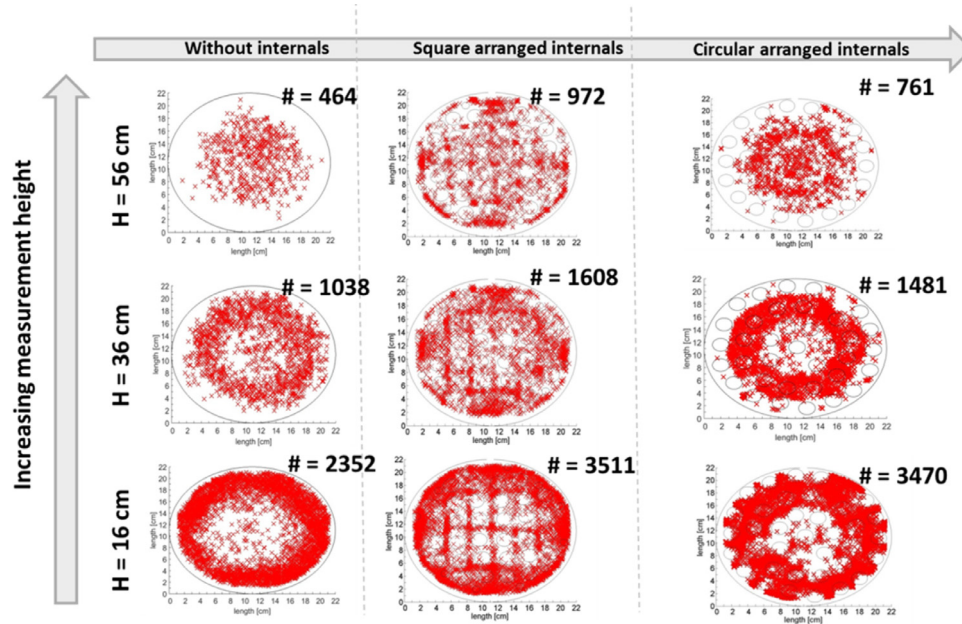


Fig. 6 Distribution of bubble centroids and number of linked bubbles at different measurement heights for a fluidization number of three, \emptyset column = 22 cm.

to be better distributed compared to the setup without internals at a measurement height of 56 cm. The presence of vertical internals, which can be an obstacle for radial bubble coalescence, may be a possible explanation for a more uniform bubble distribution as it has already been stated in Maurer et al. (2015).

Fig. 6 shows the positions of the volumetric center of gravity for all coherent void fractions that could be identified by the bubble linking algorithm. The particular numbers in Fig. 6 indicate the number of bubbles that could be linked between the lower and upper measurement planes. The pattern of the centroid positions mostly corresponds to the hold-up distribution as shown above. It has to be pointed out that the number of plotted centroids does not correspond to the number of linked bubbles. This is due to the fact that not each individual bubble which is detected at the lower measurement plane can be linked to the corresponding bubble at the upper measurement plane because of the restrictions that are defined in the bubble linking algorithm. A sensitivity study on the influence of different restrictions (e.g. threshold, minimal bubble volume, minimal bubble rise velocity, maximum displacement of the bubble centroid in radial direction) in the reconstruction algorithm on the bubble rise velocity and the bubble size was conducted in Maurer et al. (2015). The threshold value that is decisive whether a pixel is assigned to the bubble phase or to the dense phase turned out to be the most sensitive parameter on the bubble size. The optimal threshold between the bubble and the dense phase was determined to 0.63 by a calibration with air filled thin walled acrylic glass tubes that are located at known positions Maurer (2015). In order to link the bubbles, the maximum radial bubble movement for the center of gravity between both measurement planes was limited to 3 cm. This corresponds to an angle of 55° which is in the range of the distance between the centers of two internal tubes that are adjacent to each other. The minimum BRV was set to 0.1 m/s, the maximum BRV was set to 2 m/s. Furthermore, the maximum increase or decrease of the bubble volume between both measurement planes was set to a factor of two. For the setup without internals as well as with circularly arranged internals, centroids are located in an annular shape at a lower measurement plane that contracts towards higher measurement heights. However, the centroids for the quadratically ar-

ranged internals are more evenly distributed. The number of centroids is a direct indicator for the amount of detected bubbles. It becomes obvious that the density of bubble centroids decreases with an increasing measurement height due to bubble coalescence for all configurations. A decrease in the density of bubble centroids towards higher measurement heights is consistent with generally larger bubbles in the upper regions of the bed. However, it should be pointed out again that not each bubble event at the lower measurement plane can be linked to a corresponding event at the upper measurement plane for which reason also effects like a larger velocity or a stronger deformation of bubbles could influence the amount of linked bubbles. It emerges that the total number of linked bubbles at a measurement height of 16 cm for the configuration without internals is significantly lower compared to the configurations with internals. This is a strong indication that internals decrease the rate of bubble coalescence. All centroids depicted in Fig. 6 that are placed inside a tube correspond to bubbles that surround one or more internal tubes.

3.2.2. Hold-up evaluation for a fluidization number of six

Fig. 7 presents the hold-up distribution for a fluidization number of six. Evaluation of the hold-up distribution at a u/u_{mf} of six shows the expected result of a general higher hold-up due to a higher total volume flow of gas. For the setting without internals, the annular shape of the region with an increased hold-up at a measurement height of 16 cm persists. However, in contrast to a fluidization number of three, the ring is already contracted at a measurement height of 36 cm.

This finding is in agreement with the results derived by a 3-D simulation of a bubbling fluidized bed without vertical internals (Bakshi et al., 2016). The simulation has shown that the height above which the bubbles tend to rise predominantly in the middle of the column decreases with increasing fluidization number. A higher volume flow that implements a faster bubble frequency and generally larger bubbles results in an increased rate of lateral bubble coalescence which explains the sooner contraction of the annular shape. An increase of the bubble frequency for higher volume flows was as already reported in Geldart (1970).

Hold-up distribution for circularly arranged internals also depicts an annular shape of an increased hold-up that is not con-

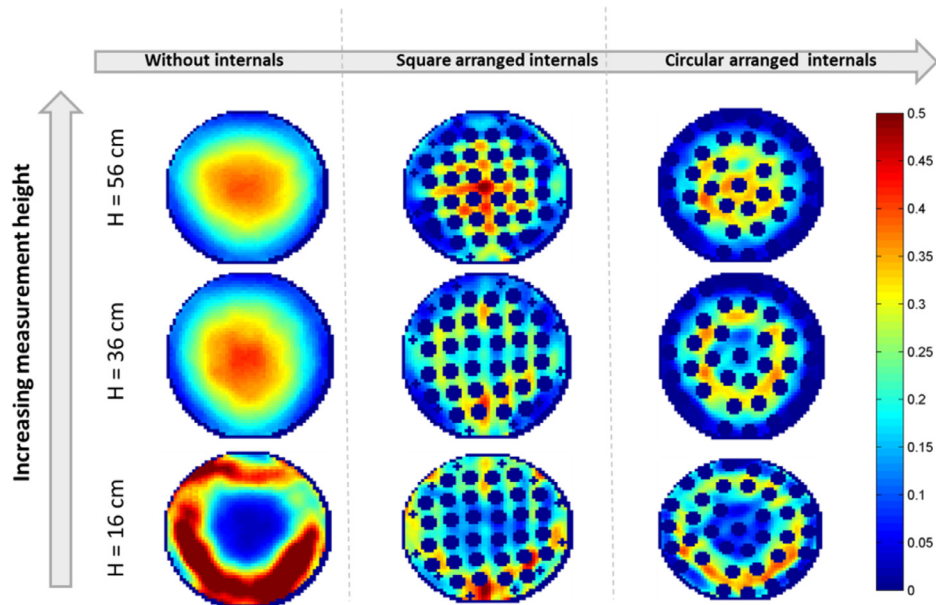


Fig. 7. Hold-up distribution at different measurement heights for a fluidization number of six, \varnothing column = 22 cm. (For interpretation of the references to color in this figure, the reader is referred to the web version of this article.)

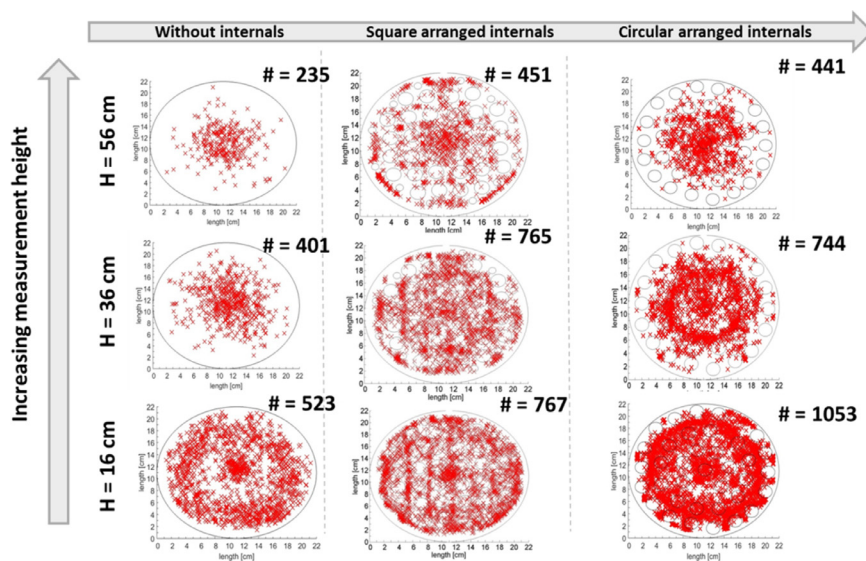


Fig. 8. Distribution of bubble centroids and number of linked bubbles at different measurement heights for a fluidization number of six.

tracted until a measurement height of 56 cm. The region around the outer ring of internals is almost free of bubbles since the internals are very close to the column wall for this setting. Circularly arranged internals show a local maximum hold-up of 40%, while the local maximum value for the setting with quadratically arranged internals is up to 50%. The absence of a central tube for the quadratically arranged setting is a possible explanation for the significant increase of the hold-up towards the center. Bubbles may coalesce unhindered in radial direction towards the center.

Fig. 8 shows the centroid positions of all coherent areas that were assigned to a bubble at the lower detector array and the number of bubbles that could be linked between the particular lower and upper measurement planes. In contrast to a fluidization number of three (confer to Fig. 6), the annular shape for the setup without internals and for circularly arranged internals contracts at a lower measurement height. Higher fluidization number generally result in larger bubbles and a higher rate of bubble coalescence

which could explain the earlier closing of the annular shape at a fluidization number of six compared to the fluidization number of three. In general, the tendency towards a lower number of bubbles without internals is confirmed.

It is noticeable for the setup with quadratically arranged internals that the number of linked bubbles at a measurement height of 16 cm is only marginally larger compared to the measurement height of 36 cm although the amount of plotted red centroids seems to decrease noticeable. This is in contrast to all other settings and may be explained by the fact that a lot of coherent voidage areas at the lower measurement plane could not be linked to an appropriate voidage area at the upper measurement plane.

3.2.3. Mean hold-up over the cross-section

The mean cross-sectional hold-up is usually taken into account for numerical models simulating a bubbling fluidized bed (Zhang et al., 2015). Fig. 9 depicts the mean hold-up in dependence of the

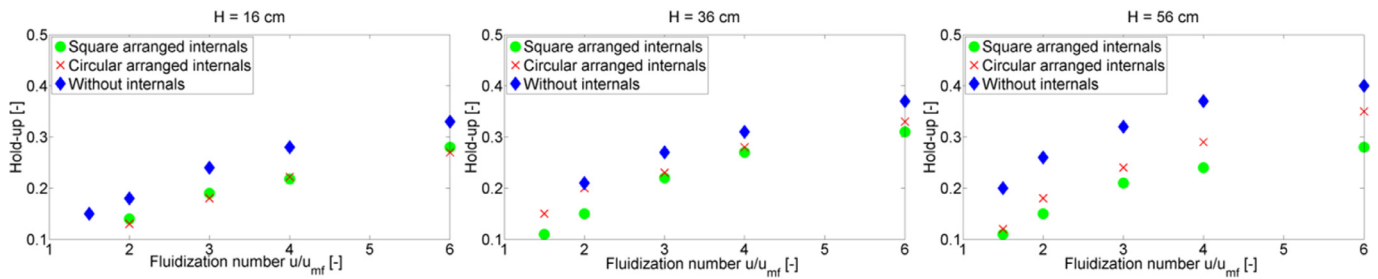


Fig. 9. Mean cross-sectional hold-up for a measurement height of 36 cm as a function of the fluidization number for a column size of 22 cm.

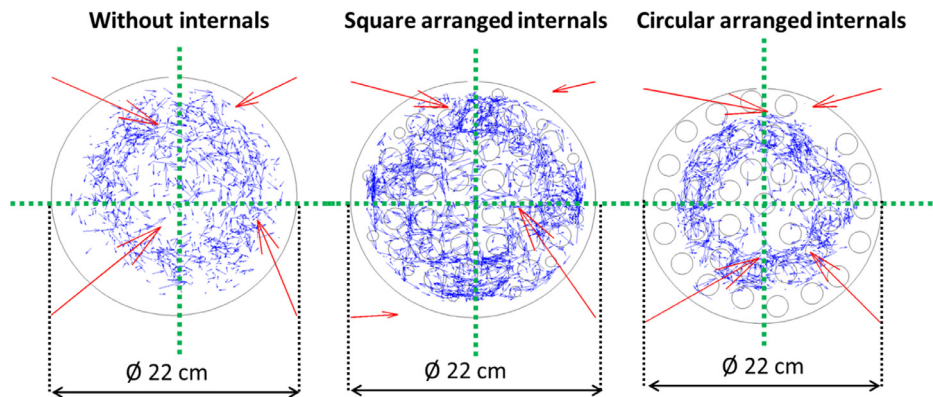


Fig. 10. Movement of bubble centroids between lower and upper measurement plane and mean movement direction of all linked bubbles for each quadrant at a measurement height of 36 cm and $u/u_{mf} = 3$ for a column size of 22 cm. (For interpretation of the references to color in this figure, the reader is referred to the web version of this article.)

fluidization number for measurement heights of 16 cm, 36 cm and 56 cm. The period of time a bubble is present at a certain pixel divided by the total measurement duration results in the time-averaged hold-up for the individual pixel. The time-averaged hold up of all pixels at one measurement plane that are not assigned to an internal result in the mean hold-up above the cross-section. For every measurement height, the configuration without internals resulted in a larger hold-up compared to the settings with internals. Only at a measurement height of 56 cm and for fluidization numbers above four, a visible difference between both configurations with internals starts to appear.

3.3. Movement of bubble centroids between lower and upper measurement plane

The reconstruction of the bubbles at the lower and upper detector arrays enables the tracking of the center of gravity between both measurement planes. Fig. 10 shows the movement of all bubble centroids (blue arrows) between the lower and upper measurement plane as well as the mean movement direction of all linked bubbles in every quadrant of the column (red arrows). The beginning of each blue arrow stands for the location of the centroid at the lower measurement plane, the end of the arrow for the position at the upper measurement plane. In order to visualize the mean movement direction (red arrows) in every quadrant, the lengths of the arrows illustrating the mean movement direction are stretched by a factor of 50. The same scale of the arrows is used for all three configurations. For the circular arrangement of internals, the toroidal shape of the moving direction exhibits a sharper border compared to the setup without internals. This is due to the fact that bubbles are almost not present in the free space between the tubes of the outer circle as already shown with the hold-up distribution in Fig. 5. As seen for the setup with the quadratically arranged internals, the main directions of movement are in the

free spaces parallel to the internal pattern. In general, the mean movement direction of the bubbles in every quadrant points into the interior of the column. This fact confirms the results presented in Figs. 5 and 6 that show an annular shaped region of an enlarged bubble hold-up and bubble centroid density that contracts towards higher measurement heights. For the configuration without internals, the annulus-shaped ring with increased hold-up contracts earlier compared to the configurations with internals as it was shown in Fig. 6. This outcome is reflected by the fact that the arrows of the mean bubble movement direction point more directly to the center of the column for the configuration without internals compared to the configurations with internals as depicted in Fig. 10.

3.3.1. Latitude angle of bubble movement

On basis of the centroid positions for the same linked bubble at the lower and upper measurement plane, a latitude angle α can be obtained which is an indicator for the radial bubble movement as illustrated in Fig. 11. Since a change in the bubble geometry may shift the centroid position, the angle is calculated based on the assumption that the bubble shape only changes marginally between both measurement planes.

The corresponding angle distribution to the bubble movement depicted in Fig. 10 is shown in Fig. 12. The mean angle of radial bubble movement without internals is slightly smaller compared to the configurations with internals. At first glance, this may be interpreted as a contradiction to the findings that internals impede the radial bubble coalescence. The shape of the distributions shown in Fig. 12 may also give a hint how the lateral bubble movement depends on the presence of internals. The histogram for the configuration without internals shows a stronger descent towards larger angles of lateral bubble movement compared to both configurations with internals.

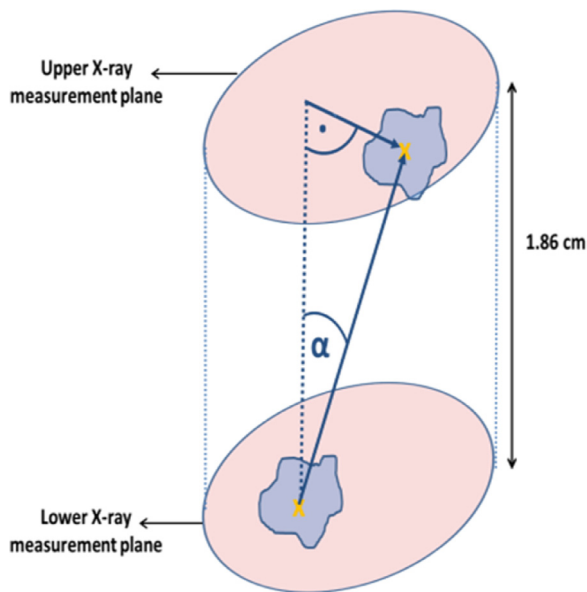


Fig. 11. Illustration of lateral movement angle between lower and upper measurement plane.

The presence of vertical internals in the column could be the reason for a more pronounced radial bubble movement compared to the setting without internals. For the configuration with vertical internals, bubbles with a horizontal movement component may have to push their entire bubble volume through the “bottle-neck” between two internal tubes. This leads to a larger horizontal movement distance compared to the configuration without internals where no geometrical constrictions are present. For example, a horizontal shift of 2 cm which corresponds to the diameter of one vertical tube, yields in a lateral angle of 47° .

A more pronounced radial bubble movement may support the particle mixing; a desired behavior with regard to internal catalyst regeneration in a BFB reactor. Computer simulations based on a two-fluid model have already shown that ring-shaped baffles enhance the particle mixing as shown by means of a 2-D model in Hosseini et al. (2009).

3.4. X-ray measurements of the bubble size and bubble rise velocity

Especially for the setup with internals, bubbles do not occur in a perfectly round shape as depicted in Figs. 3 and 4. To obtain comparable results, the bubble size is often described by the volume equivalent spherical bubble diameter $d_{b,eq}$ in literature. Information on the bubble size and bubble rise velocity is an important key to develop correlations that predict the bubble behavior inside

a BFB whereof many are available in the open literature (Maurer et al., 2016; Mori and Wen, 1975; Horio and Nonaka, 1987; Hillgardt and Werther, 1987).

The number weighted mean volume equivalent bubble diameter is shown in Fig. 13 at measurement heights of 16 cm, 36 cm and 56 cm for all three internals configurations. Without the vertical internals present in the BFB, the mean volume equivalent diameter almost reaches twice the diameter compared to the setup with internals. As already discussed in the previous sections, vertical internals may form an obstacle to radial bubble coalescence. A higher rate of bubble coalescence is therefore given for the configuration without internals resulting in a larger mean bubble size. The mean equivalent bubble diameter for quadratically arranged and circularly arranged internals approximately lies in the same range with a slight tendency towards larger bubbles for the circular arrangement at higher measurement heights.

Although the mean bubble diameter is often used to predict the mass transfer rate in a BFB (Sit and Grace, 1981), the fraction of larger bubbles within bubble size distribution is the limiting factor for the mass transfer between the bubble phase and the dense phase. Histograms provide a possibility to present the range of the bubble size distribution as depicted in Fig. 14. Since both internals configurations have a similar effect on the bubble size, only the results for the setup with quadratically arranged internals and without internals are compared in the following histograms for the sake of clarity.

It emerges that for the configurations with internals, the fraction of bubbles with an equivalent diameter smaller than 5 cm remains constantly high for all investigated fluidization numbers and measurement heights. For the setting without internals and at a measurement height of 56 cm, the majority of bubbles have a volume equivalent diameter above 15 cm which is a clear sign that the bubbles appear in the shape of slugs.

For a measurement height of 56 cm and a fluidization number of six, a second peak is indicated for the configuration with internals. This peak can be interpreted as the onset of the slugging regime, however, the peak is less pronounced compared to the setting without internals. The onset of an undesired slugging regime may therefore not be totally suppressed by the presence of vertical internals, but, it is shifted towards higher fluidization numbers and measurement heights.

Fig. 15 depicts the mean number based BRV for the same experimental conditions as shown above for the mean BS. The tendency towards faster bubbles without internals is obvious, although, the relative deviation between the BRV for the configuration with and without internals is less pronounced compared to the mean volume equivalent bubble diameter shown in Fig. 13.

In terms of reactor performance, fast and at the same time large bubbles may cause a problem since they promote a breakthrough

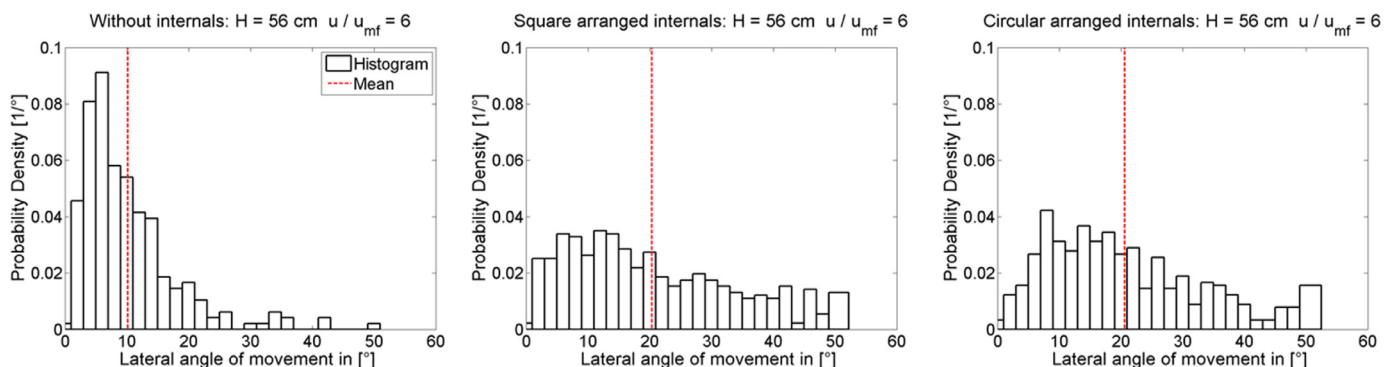


Fig. 12. Latitude angle distribution for different internal configurations.

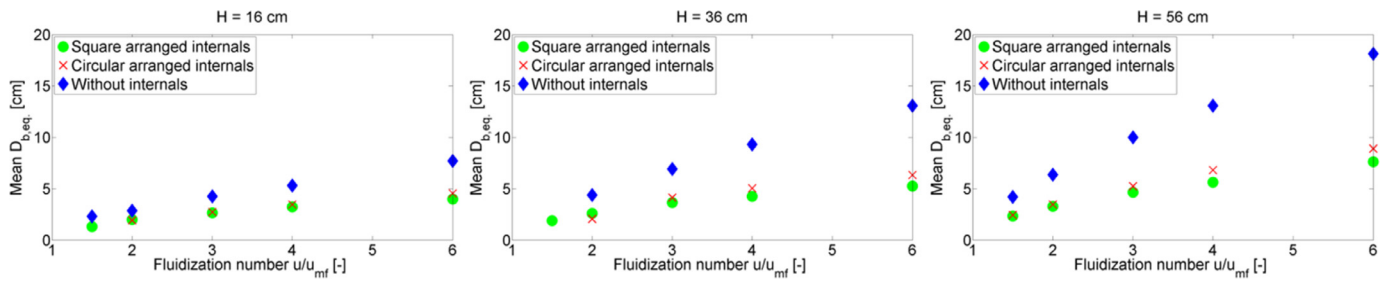


Fig. 13. Number weighted mean volume equivalent bubble diameter as a function of the fluidization number for a column size of 22 cm.

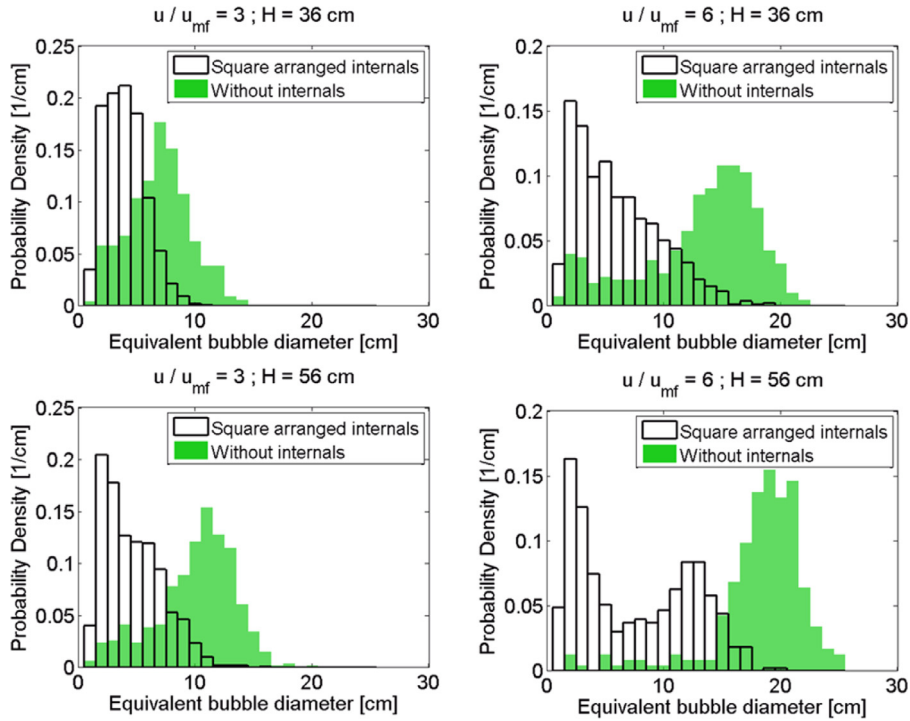


Fig. 14. Histograms of volume equivalent bubble diameters for a column size of 22 cm.

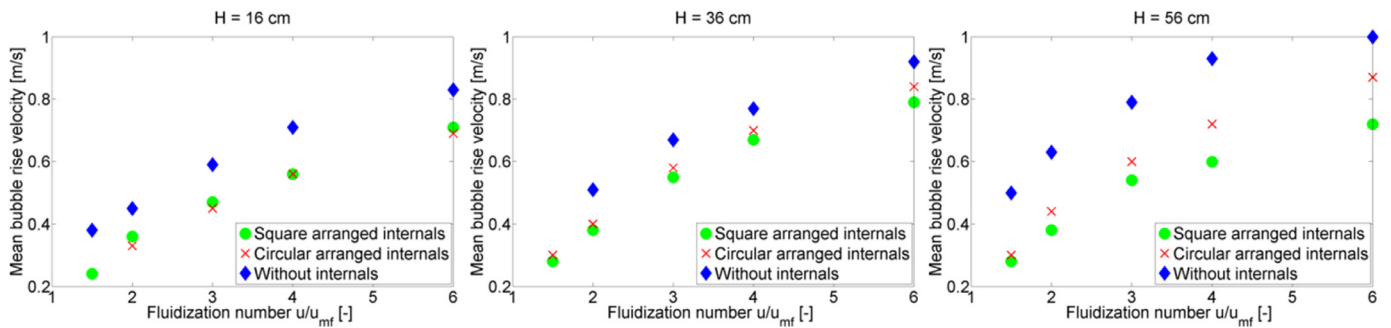


Fig. 15. Number based mean bubble rise velocity as a function of the fluidization number for a column size of 22 cm.

of reactants due to an insufficient mass transfer from the bubble to the dense phase where the catalyst is located. Fig. 16 shows the bubble rise velocity of all detected bubbles in dependence of the equivalent bubble diameter for a fluidization number of six at a measurement height of 36 cm and 56 cm above the distributor plate. The plot indicates a larger BS and BRV for the setup without internals whereas the presence of internals results in generally smaller and slower bubbles.

Fig. 17 compares the amount of linked bubbles for the settings without internals and with quadratically arranged internals in de-

pendence of the bubble size and bubble rise velocity at a measurement height of 36 cm and a fluidization number of six. The setup with internals shows a clear tendency towards a larger number of bubbles for a decreasing bubble size and bubble rise velocity. Without internals, an increased number of bubbles are located in an area around a BRV of 0.5 m/s and a BS of 15 cm. Yet, the peak is less pronounced compared to the setup with internals. For the setting with internals, fast bubbles with a BRV of up to 1.5 m/s possess by the majority a maximum BS of 7 cm. In contrast, many fast bubbles have a BS of up to 15 cm for the setting without in-

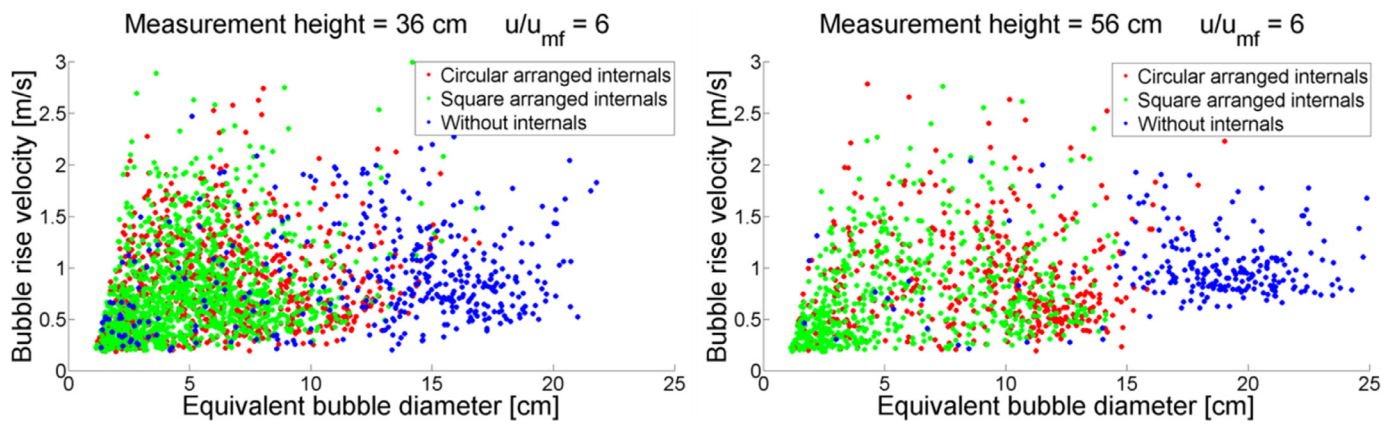


Fig. 16. Bubble rise velocity in dependence of the equivalent bubble diameter for the three internal configurations for a column size of 22 cm.

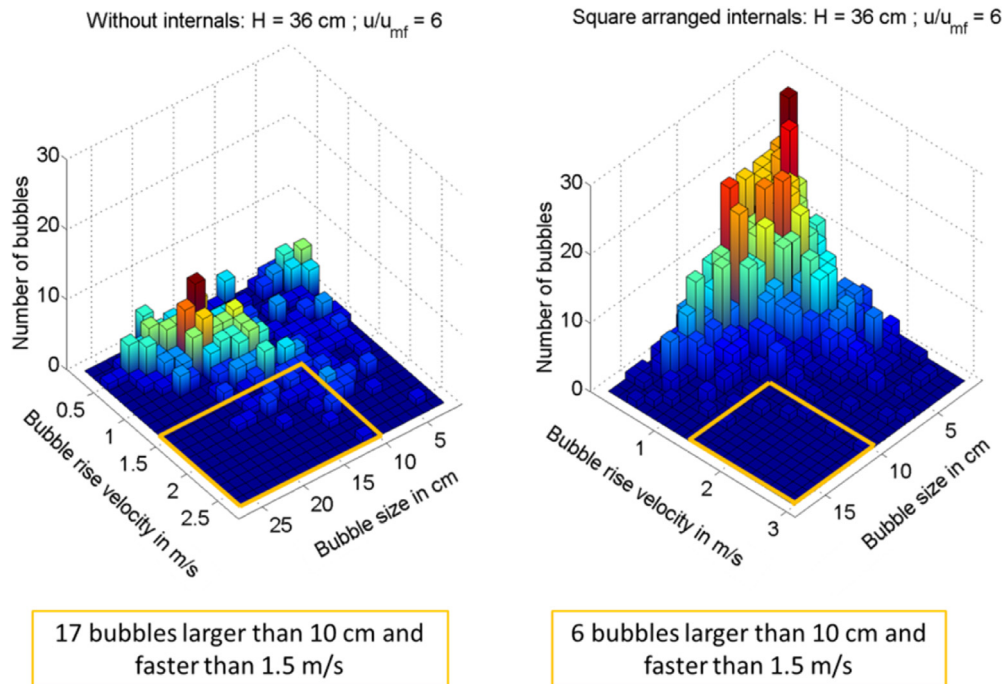


Fig. 17. 3-D histogram of bubble number in dependence of bubble size and bubble rise velocity for configuration without and with quadratically arranged internals for a column size of 22 cm.

ternals. In total, there are almost three times more bubbles in a critical region above a volume equivalent diameter of 10 cm and at the same time a velocity above 1.5 m/s for the configuration without internals compared to the configuration with vertical internals as depicted in Fig. 17. Hence, it can be stated that the fraction of educts flowing through a bubbling fluidized bed reactor without reaction may be reduced by means of vertical internals.

3.5. Influence of column diameter on bubble size and bubble rise velocity

The scale-up of bubbling fluidized bed technology is an ongoing challenge since the procedure is often based on empirical values (Knowlton et al., 2005). Usually, the full set of Glicksman's (1984) scaling relations based on dimensionless numbers is used to transfer the results of pilot plants into larger dimensions. However, hydrodynamic measurements with columns of different diameters may have to support the scale-up process since there is a lack of data to verify predictions, especially in the range of larger columns (Sanderson and Rhodes, 2005).

The subsequently presented results for the column with a diameter of 14 cm as well as the corresponding X-ray measurement setup have already been published in Maurer et al. (2015). In Fig. 18, the mean equivalent bubble diameter with and without internals is shown in dependence of the column diameter for fluidization numbers of three and four. Towards upper measurement heights, it emerges that the difference in the bubble size between the smaller and larger columns does not get too large for the configuration with internals. Without internals, the mean bubble size is significantly larger at a fluidization number of four for the column with a \emptyset of 22 cm compared to the mean bubble size of the column with a \emptyset of 14 cm. Experimental investigations on a sectoral scale-up approach with vertical internals were already conducted by means of an optical measurement technique in the scope of Maurer et al. (2014) and support the conclusion of this work that the scale-up process can be facilitated if vertical internals are present since bubbles are only marginally larger in columns with a wider diameter if vertical internals are present.

Fig. 19 shows the mean BRV with and without internals for the column diameters of 14 cm and 22 cm. In contrast to the mean vol-

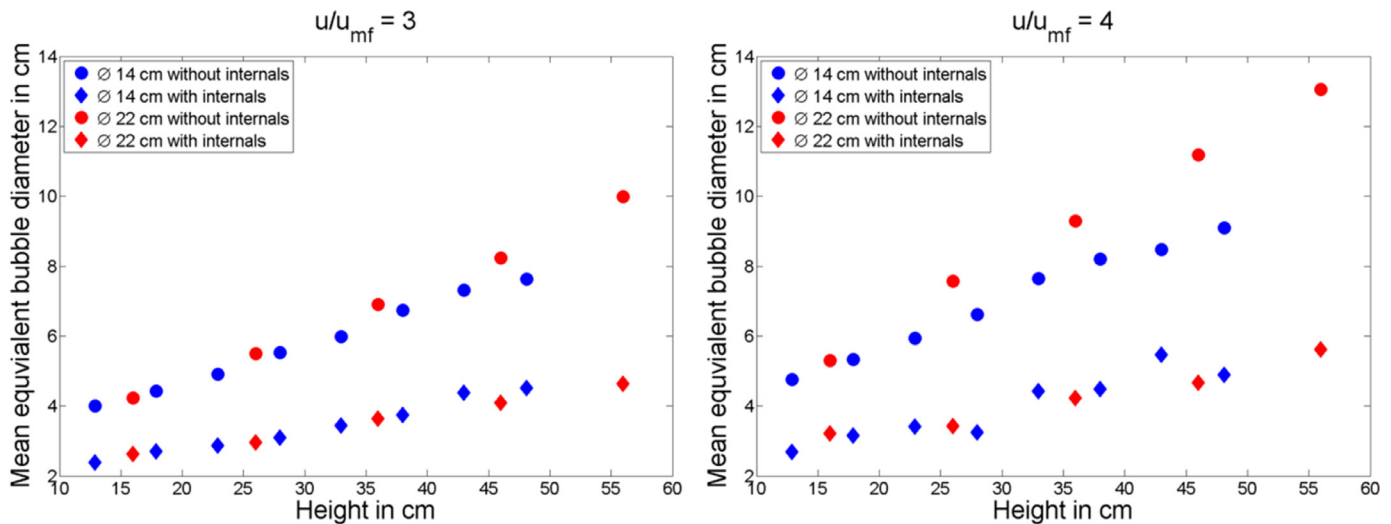


Fig. 18. Comparison of mean equivalent bubble diameter between \varnothing 14 cm and \varnothing 22 cm columns.

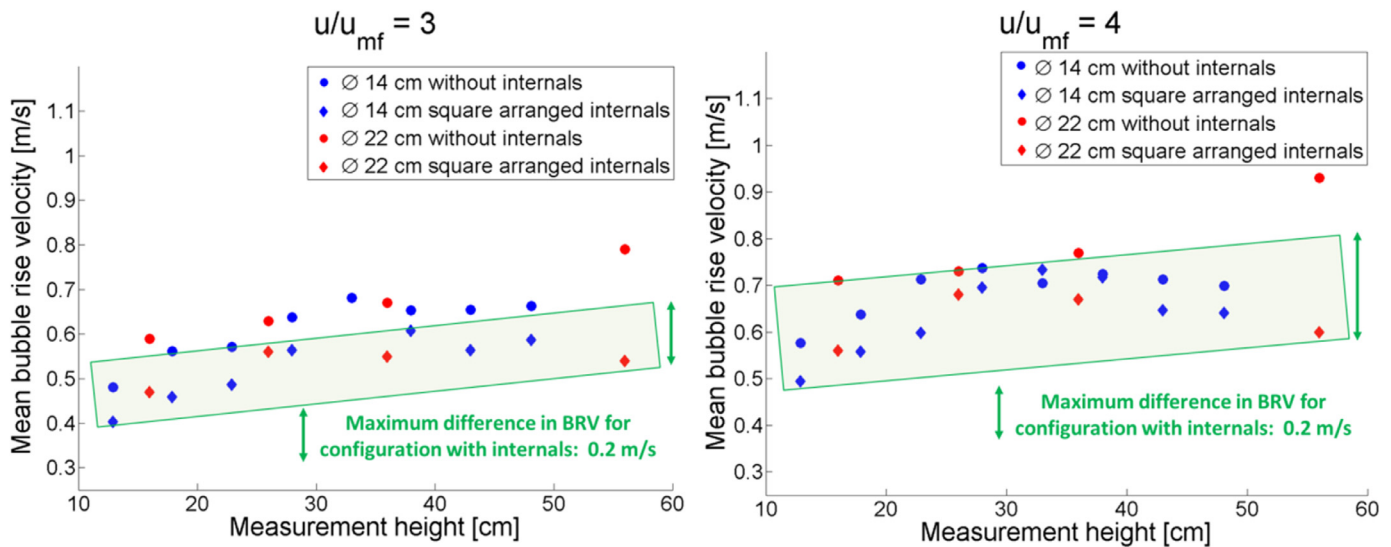


Fig. 19. Comparison of the mean BRV between \varnothing 14 cm and \varnothing 22 cm columns at fluidization numbers of 3 and 4.

ume equivalent diameter shown in Fig. 18, no clear trend can be identified except for the column with a diameter of 22 cm without internals for which the BRV increases constantly towards higher measurement heights. For this configuration, less pronounced wall effects due to the absence of internals and a larger column diameter could be a possible explanation for the steady increase of the BRV. For identical fluidization numbers and measurement heights, the bubble rise velocity only varies in a range of maximum 0.2 m/s between the columns with a diameter of 14 cm and 22 cm for the configuration with internals which is depicted by the underlying box shown in Fig. 19.

There are no experimental data points available for a measurement height of 56 cm at the column with a diameter of 14 cm. However, the bubble rise velocity tends to increase only marginally at measurement heights above 20 cm for the investigated column with 14 cm in diameter without internals at fluidization numbers of three and four (Maurer et al., 2015). Under the assumption that this trend continues, a large deviation in the bubble rise velocity between the smaller and the larger column at measurement heights above 50 cm could be expected if no vertical internals are present.

Therefore, it can be concluded that the column diameter has a negligible impact on the mean BRV if vertical internals are present, a fact that has already been investigated by a sectoral scaling approach in Maurer et al. (2014).

In summary, it can be emphasized that the scale-up procedure of bubbling fluidized beds gets less critical if vertical internals are present. Towards higher measurement heights, the increase of the bubble rise velocity is limited and the growth of the bubble size is not very pronounced due to the presence of internals. The difference in the bubble properties for similar measurement heights and fluidization number between the smaller and the larger column decreases if vertical internals are present.

This allows a scale-up of bubbling fluidized beds without running the risk that the majority of bubbles are fast and at the same time large.

4. Conclusions

The hydrodynamic behavior of a cold-flow bubbling fluidized bed with a diameter of 22 cm was investigated by means of X-ray tomography and compared to the results for a bubbling fluidized

bed with a diameter of 14 cm. The measurements at the column with a diameter of 22 cm were conducted at different fluidization numbers and heights for two geometrical configurations of vertical internals as well as for a column without internals.

The evaluation of the bubble hold-up showed that for lower measurement heights, an increased hold-up is present in an annulus-shaped region which contracts towards higher measurement heights. It emerged that the mean latitudinal angle of horizontal bubble movement was slightly larger for the configuration with internals compared to the configuration without internals. One possible explanation could be that bubbles have to pass through the constricted opening between the internals if bubbles contain a horizontal movement component while they ascend.

Furthermore, the effect of vertical internals on the mean bubble size and the mean bubble rise velocity was investigated for the column with a diameter of 22 cm and compared to the results of the column with a diameter of 14 cm. If vertical internals are present, it could be shown that the column diameter has only a minor influence on the bubble size. Additionally, the bubble rise velocity for the configurations with internals is almost not affected by the column diameter. In summary, it can be stated that the scale-up process from pilot plants to an industrial scale may be simplified if vertical internals are present.

The hydrodynamic results for a column with quadratically arranged internals are compared to the hydrodynamic results for a column with circularly arranged internals. It emerged that the geometrical arrangement of the vertical internals does almost not affect the volume equivalent bubble diameter and the bubble rise ve-

locity. Slight differences in terms of the bubble distribution on the cross-section were detected between the different geometric arrangements of internals. Quadratically arranged internals have the benefit that the majority of the bubbles are spread over a broader part of the cross-section compared to the circle-like arrangement of internals for which the outer region of the column is almost free of bubbles. For higher measurement heights, however, the configuration with quadratically arranged internals shows an undesired high locally hold-up in the middle of the column since there is no central tube present for this configuration.

The minor influence of the internals arrangement on the hydrodynamics allows the conclusion that results which are obtained from a non-square arrangement of the internals can be transferred to a configuration where the internals are arranged in squares. A configuration of quadratically arranged heat exchanger tubes is often used for industrial applications due to an easier manufacturing process. The results of the X-ray measurements may also be applied to validate existing computer models simulating the flow characteristics of a bubbling fluidized bed with vertical internals (Verma et al., 2016).

Acknowledgments

The support of the Swiss Competence Center for Energy Research on Biomass (Biosweet) is gratefully acknowledged.

Appendix

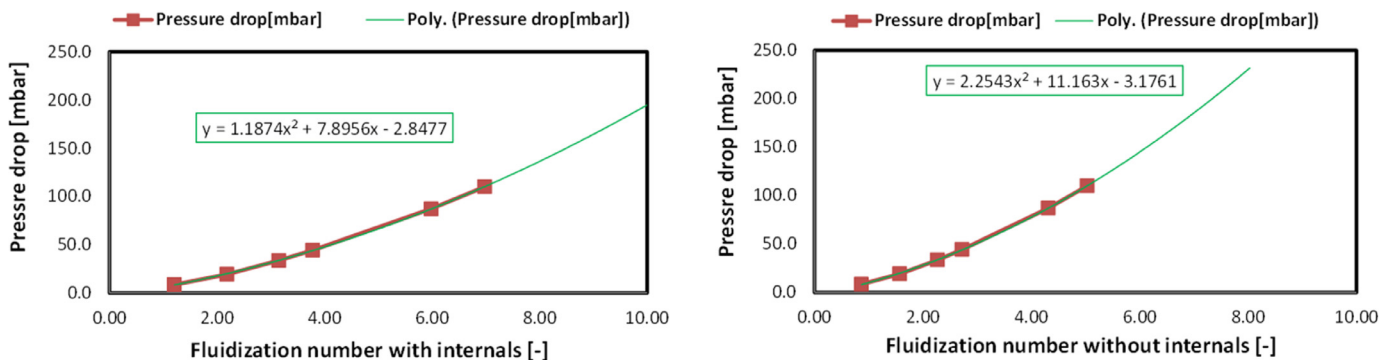


Fig. 20. Measured pressure drop above the distributor plate in dependence of the fluidization number.

References

- Acosta-Iborra, A., Sobrino, C., Hernandez-Jimenez, F., de Vega, M., 2011. Experimental and computational study on the bubble behavior in a 3-D fluidized bed. *Chem. Eng. Sci.* 66 (15), 3499–3512.
- Andersen, A.H., Kak, A.C., 1984. Simultaneous algebraic reconstruction technique (SART): A superior implementation of the art algorithm. *Ultrasound Imaging* 6 (1), 81–94.
- Bakshi, A., Altantzis, C., Bates, R.B., Ghoniem, A.F., 2016. Study of the effect of reactor scale on fluidization hydrodynamics using fine-grid (CFD) simulations based on the two-fluid model. *Powder Technol.* 299, 185–198.
- Baskakov, A.P., Tuonogov, V.G., Filippovsky, N.F., 1986. A study of pressure fluctuations in a bubbling fluidized bed. *Powder Technol.* 45 (2), 113–117.
- Beetstra, R., Nijenhuis, J., Ellis, N., van Ommen, J.R., 2009. The influence of the particle size distribution on fluidized bed hydrodynamics using high-throughput experimentation. *AIChE J.* 55 (8), 2013–2023.
- Geldart, D., 1970. The size and frequency of bubbles in two- and three-dimensional gas-fluidized beds. *Powder Technol.* 4 (1), 41–55.
- Glicksman, L.R., 1984. Scaling relationships for fluidized beds. *Chem. Eng. Sci.* 39 (9), 1373–1379.
- Gunn, D.J., Hilal, N., 1996. Heat transfer from vertical inserts in gas-fluidized beds. *Int. J. Heat Mass Transf.* 39 (16), 3357–3365.
- Hillgardt, K., Werther, J., 1987. Influence of temperature and properties of solids on the size and growth of bubbles in gas fluidized beds. *Chem. Eng. Technol.* 10 (1), 272–280.
- Horio, M., Nonaka, A., 1987. A generalized bubble diameter correlation for gas–solid fluidized beds. *AIChE J.* 33 (11), 1865–1872.
- Hosseini, S., Rahimi, R., Zivdar, M., Samimi, A., 2009. The effect of ring baffles on the hydrodynamics of a gas–solid bubbling fluidized bed using computational fluid dynamics. *Proc. Inst. Mech. Eng. Part C J. Mech. Eng. Sci.* 223 (10), 2281–2289.
- Kim, S.W., Ahn, J.Y., Kim, S.D., Lee, D.H., 2003. Heat transfer and bubble characteristics in a fluidized bed with immersed horizontal tube bundle. *Int. J. Heat Mass Transf.* 46 (3), 399–409.
- Knowlton, T.M., Karri, S.B.R., Issangya, A., 2005. Scale-up of fluidized-bed hydrodynamics. *Powder Technol.* 150 (2), 72–77.
- Kopyscinski, J., Schildhauer, T.J., Biollaz, S.M.A., 2009. Employing catalyst fluidization to enable carbon management in the synthetic natural gas production from biomass. *Chem. Eng. Technol.* 32 (3), 343–347.
- Kumar, S.B., Moslemian, D., Duduković, M.P., 1997. Gas-holdup measurements in bubble columns using computed tomography. *AIChE J.* 43 (6), 1414–1425.
- Kunii, D., Levenspiel, O., 1968. Bubbling bed model. Model for flow of gas through a fluidized bed. *Ind. Eng. Chem. Fundam.* 7 (3), 446–452.
- Kunii, D., Levenspiel, O., 2013. *Fluidization Engineering*. Elsevier.
- Latham, R., Pottert, O.E., 1970. Back-mixing of gas in a 6-in diameter fluidized bed. *Chem. Eng. J.* 1 (2), 152–162.
- Maurer, S., Schildhauer, T.J., van Ommen, J.R., Biollaz, S.M.A., Wokaun, A., 2014. Scale-up of fluidized beds with vertical internals: Studying the sectoral approach by means of optical probes. *Chem. Eng. J.* 252, 131–140.
- Maurer, S., Wagner, E.C., van Ommen, J.R., Schildhauer, T.J., Teske, S.L., Biollaz, S.M.A., Wokaun, A., Mudde, R.F., 2015a. Influence of vertical internals on a bubbling fluidized bed characterized by X-ray tomography. *Int. J. Multiph. Flow* 75, 237–249.
- Maurer, S., Wagner, E.C., Schildhauer, T.J., van Ommen, J.R., Biollaz, S.M.A., Mudde, R.F., 2015b. X-ray measurements of bubble hold-up in fluidized beds with and without vertical internals. *Int. J. Multiph. Flow* 74, 118–124.
- Maurer, S., Gschwend, D., Wagner, E.C., Schildhauer, T.J., van Ommen, J.R., Biollaz, S.M.A., Mudde, R.F., 2016. Correlating bubble size and velocity distribution in bubbling fluidized bed based on X-ray tomography. *Chem. Eng. J.* 298, 17–25.
- Maurer, S., 2015. Hydrodynamic Characterization and Scale-up of Bubbling Fluidized Beds for Catalytic Conversion. Eidgenössische Technische Hochschule ETH Zürich, ETH Zürich, Dissertation Nr. 22722.
- Mori, S., Wen, C.Y., 1975. Estimation of bubble diameter in gaseous fluidized beds. *AIChE J.* 21 (1), 109–115.
- Mudde, R.F., 2010. Time-resolved X-ray tomography of a fluidized bed. *Powder Technol.* 199 (1), 55–59.
- Mudde, R.F., 2011. Bubbles in a fluidized bed: a fast X-ray scanner. *AIChE J.* 57 (10), 2684–2690.
- Natale, F.D., Bareschino, P., Nigro, R., 2010. Heat transfer and void fraction profiles around a horizontal cylinder immersed in a bubbling fluidized bed. *Int. J. Heat Mass Transf.* 53 (17–18), 3525–3532.
- Rüdisüli, M., Schildhauer, T.J., Biollaz, S.M.A., van Ommen, J.R., 2012a. Bubble characterization in a fluidized bed by means of optical probes. *Int. J. Multiph. Flow* 41, 56–67.
- Rüdisüli, M., Schildhauer, T.J., Biollaz, S.M.A., Wokaun, A., van Ommen, J.R., 2012b. Comparison of bubble growth obtained from pressure fluctuation measurements to optical probing and literature correlations. *Chem. Eng. Sci.* 74, 266–275.
- Rüdisüli, M., Schildhauer, T.J., Biollaz, S.M.A., van Ommen, J.R., 2012c. Bubble characterization in a fluidized bed with vertical tubes. *Ind. Eng. Chem. Res.* 51 (12), 4748–4758.
- Rüdisüli, M., 2012. Characterization of Rising Gas Bubbles in Fluidized Beds by Means of Statistical Tools. ETH/PSI.
- Rautenbach, C., Melaan, M.C., Halvorsen, B.M., 2013. Statistical diagnosis of a gas–solid fluidized bed using electrical capacitance tomography. *Int. J. Multiph. Flow* 49, 70–77.
- Sanderson, J., Rhodes, M., 2005. Bubbling fluidized bed scaling laws: evaluation at large scales. *AIChE J.* 51 (10), 2686–2694.
- Sasic, S., Leckner, B., Johnsson, F., 2005. Fluctuations and waves in fluidized bed systems: the influence of the air-supply system. *Powder Technol.* 153 (3), 176–195.
- Seemann, M.C., Schildhauer, T.J., Biollaz, S.M.A., Stucki, S., Wokaun, A., 2006. The regenerative effect of catalyst fluidization under methanation conditions. *Appl. Catal. A Gen.* 313 (1), 14–21.
- Sit, S.P., Grace, J.R., 1981. Effect of bubble interaction on interphase mass transfer in gas fluidized beds. *Chem. Eng. Sci.* 36 (2), 327–335.
- Staub, F., 1979. Solids circulation in turbulent fluidized beds and heat transfer to immersed tube banks. *J. Heat Transf.* 101 (3), 391–396.
- Valenzuela, J.A., Glicksman, L.R., 1985. Gas flow distribution in a bubbling fluidized bed. *Powder Technol.* 44 (2), 103–113.
- van Ommen, J.R., Mudde, R.F., 2007. Measuring the gas–solids distribution in fluidized beds – a review. In: *Proceedings of the Twelfth International Conference on Fluidization – New Horizons in Fluidization Engineering*.
- Verma, V., Li, T., Dietiker, J.-F., Rogers, W.A., 2016. Hydrodynamics of gas–solids flow in a bubbling fluidized bed with immersed vertical U-tube banks. *Chem. Eng. J.* 287, 727–743.
- Werther, J., 1974. Influence of the bed diameter on the hydrodynamics of gas fluidized beds. *AIChE Symp. Ser.* 70 (141), 53–62.
- Whitemarsh, E.A., Escudero, D.R., Heindel, T.J., 2016. Probe effects on the local gas holdup conditions in a fluidized bed. *Powder Technol.* 294, 191–201.
- Yerushalmi, J., Cankurt, N.T., 1979. Further studies of the regimes of fluidization. *Powder Technol.* 24 (2), 187–205.
- Zhang, Y., Ye, M., Zhao, Y., Gu, T., Xiao, R., Liu, Z., 2015. Emulsion phase expansion of Geldart particles in bubbling fluidized bed methanation reactors: a CFD-DEM study. *Powder Technol.* 275, 199–210.